

# Department of Mathematics and Statistics

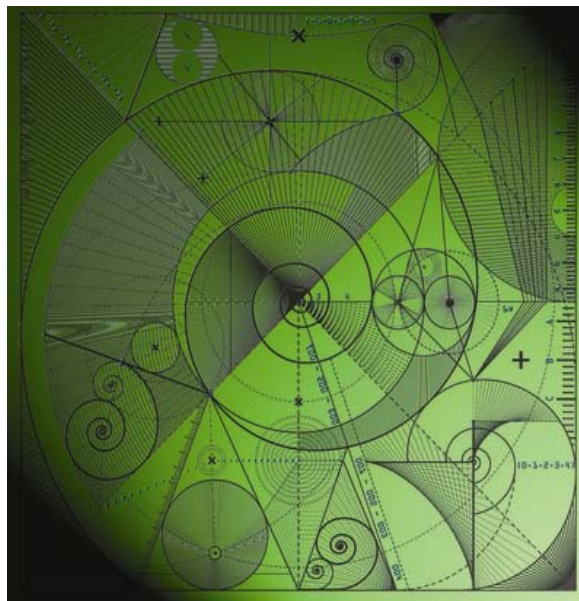
Preprint MPS-2011-17

19 October 2011

## Limits to Predicting Predictability: A case study

by

Reason L. Machete



# Limits to Predicting Predictability: A case study

R. L. Machete<sup>1</sup>

Dept. of Mathematics and Statistics, P. O. Box 220, Reading, RG6 6AX

## Abstract

It has been argued that Lyapunov exponents as a measure of predictability are of limited value because they only provide a global average. Characterising an attractor by a distribution of times for initial uncertainties to increase by a factor of  $q$  has been suggested as a more useful alternative. These have found favour in some applications, despite assumptions of the fictitious perfect model scenario. Here, an electronic circuit, which offers a good test-bed for addressing predictability in the imperfect model scenario, is presented. Implications of model imperfection on characterising the dynamics of chaotic systems are discussed.

**Keywords:** bifurcation; chaotic circuits; forecasting; radial basis functions; uncertainty

## 1 Introduction

It has been argued in [1] that Lyapunov exponents as a measure of predictability are of limited value because they only provide a global average. They would be of value if predictability was uniform over an entire attractor. For chaotic systems, it is known that this is not the case. Characterising an attractor by a distribution of times for initial uncertainties to increase by a factor of  $q$  has been suggested as a more useful alternative [1]. In the perfect model scenario, these provide information about regional losses in predictability of the underlying flow. Contrary to [2], when the model is imperfect regional losses in predictability are not an indication of the instability of the underlying flow. A model could be imperfect in either of two ways. In the first case, one may have the correct model class but uncertain about the correct parameter values. In the second case, one does not have the correct model class. This case has been termed model inadequacy [3, 4]. It limits our ability to know the current state and forecast the future. In this paper, the limitations of trying to characterise the predictability of chaotic systems when the underlying model is imperfect are elucidated. The models considered are of good forecasting quality, able to track the dynamics for at least half an oscillation.

An electronic circuit is used as a test-bed. This electronic circuit is presented here. Familiarity with basic electronics and symbols shall be assumed. A straight forward application of Kirchhoff's current laws suggests that the circuit corresponds to the Moore-Spiegel (M-S) system [5] at non-classical parameter values, which as far as we are aware, have never been considered before. With one parameter fixed, perturbing the other

---

<sup>1</sup>Corresponding author: email: [r.l.machete@reading.ac.uk](mailto:r.l.machete@reading.ac.uk), tel: +44(0)118 378 5016

Abbreviations: Moore-Spiegel (M-S); European Centre for Medium-Range Weather Forecasts (ECMWF); Radial Basis Functions (RBFs)

parameter yields a bifurcation transition sequence that has a chaotic window. The transition sequence differs from the classical one that is given in [6], assuming a rescaling of the classical parameters by 10. Moreover, data obtained from the circuit indicates some disparity with the M-S system at relevant parameter values.

Eliciting the M-S system parameter values that yield the best forecasting performance according to the Euclidean norm results in a system that always settles on a periodic orbit. Although this approach may be considered to be straight forward, the results highlight that the problem could be due to model inadequacy. Even though the model appears to forecast the circuit well for some initial conditions, it goes astray very quickly for certain initial conditions.

A natural alternative to using the M-S system to forecast the circuit evolution is to turn to radial basis functions (RBFs) models. These are especially useful when the underlying dynamics are low dimensional. Acknowledging that all these are imperfect, we compute estimates of predictability variations for the battery of models. The findings have positive implications for the forecasting of chaotic systems, highlighting the hurdles that need to be overcome when the model is imperfect.

Previous work that considered predictability in the imperfect model scenario was done by Khade & Hansen [3]. In their case, however, they used simulations of the Ikeda map rather than data from a real system. They also used singular values of linear propagators, each computed over some uniform optimisation time. An obvious point of departure is that this paper considers data from a real system. We also use times for initial uncertainties to increase by some integer factor to estimate the predictability of the underlying system. If the factor is four, we have quadrupling times. An advantage of quadrupling times over singular values is that they provide information of how initial uncertainties actually evolve over time. The limitations of performing parametric perturbations to explore model uncertainty are highlighted.

This paper is organised as follows: The next section presents the circuit that is central to the computations in this paper. A model of the circuit that is based on Kirchhoff's current laws and ideal component assumptions is presented. The model is then linked to the non-dimensional M-S system of equations. Numerical simulations of the M-S system and its perturbed version are then compared to the circuit. The framework for characterising the predictability of chaotic systems is discussed in § 3. The RBF models considered in this paper are presented in § 4. We present the results in § 5. A discussion of the results in the context of the wider literature is given in § 6. Concluding remarks are given in § 7.

## 2 The Circuit

In this section we present the circuit that is used as a test-bed in this paper. The circuit is shown in figure 1, where  $R$ ,  $R_i$ ,  $i = 1, \dots, 7$  are resistors,  $C$ 's are capacitors, and  $V_i$ ,  $i = 1, \dots, 3$  are voltages. By applying Kirchhoff's current laws and assuming ideal components, we obtain the following system of equations:

$$\begin{aligned}
 R_1 C \frac{dV_1}{dt} &= V_2, \\
 R_2 C \frac{dV_2}{dt} &= -V_2 + \frac{R_2}{R_3} V_1 - \frac{R_7 R_2}{R_4 R} (V_1 + V_3) - \frac{R_2}{10 R_5} V_1 V_3^2, \\
 R_6 C \frac{dV_3}{dt} &= V_1.
 \end{aligned} \tag{1}$$

For some scalar,  $\sigma$ , and time scale  $\tau$ , we let  $\sigma R_1 C = R_2 C = R_6 C = \tau$ . These correspond to the perturbed Moore-Spiegel equations [5]:

$$\begin{aligned} \dot{x} &= \delta y, \\ \dot{y} &= -y + \Gamma x - \gamma(x + z) - \Gamma x z^2, \\ \dot{z} &= x, \end{aligned} \quad (2)$$

For the classical M-S system,  $\delta = 1$ , which imposes the condition that

$$\frac{\Gamma}{\sigma} = \frac{R_2}{R_3} = \frac{R_2}{10R_5}. \quad (3)$$

The parameter  $\delta$  account for uncertainty about component values. For the case  $0k\Omega \leq R_7 \leq 5k\Omega$  and  $R_2 = R_4$ , we get  $\gamma \in [0, \sigma/2]$  provided  $\delta = 1$ . The classical M-S parameter values,  $\Gamma = 100$  and  $0 < \gamma < 50$ , correspond to  $R_1 = 1k\Omega$  (or  $\sigma = 100$ ) and the rest of the component values as shown in table 1. On the other hand, if instead  $R_1 = 10k\Omega$  (or  $\sigma = 10$ ) the non-dimensional model of the circuit is given by the M-S system with parameter values  $\Gamma = 10$  and  $0 < \gamma < 5$ . When  $\delta \neq 1$ , we have the perturbed M-S system of equations.

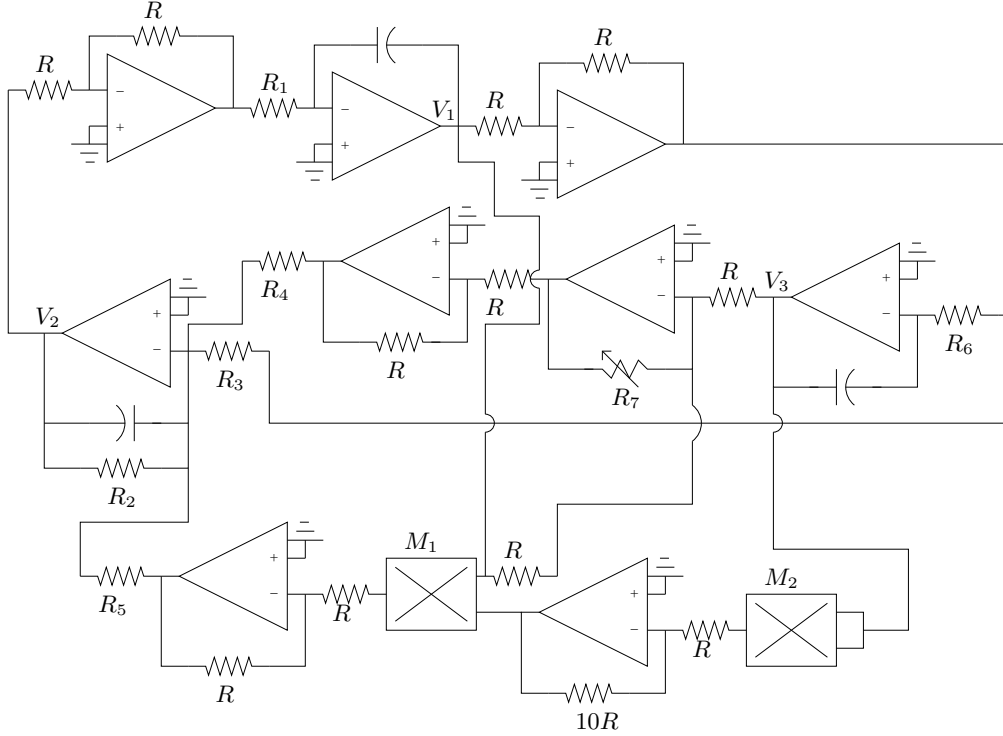


Figure 1: Circuit diagram whose ideal component model is the M-S system.

$R = 10k\Omega$	$0 \leq R_1 \leq 10k\Omega$	$R_2 = 100k\Omega$
$R_3 = 100k\Omega$	$R_4 = 100k\Omega$	$R_5 = 10k\Omega$
$R_6 = 100k\Omega$	$0 \leq R_7 \leq 5k\Omega$	$C = 10nF$

Table 1: Table of component values used in the circuit shown in figure 1.

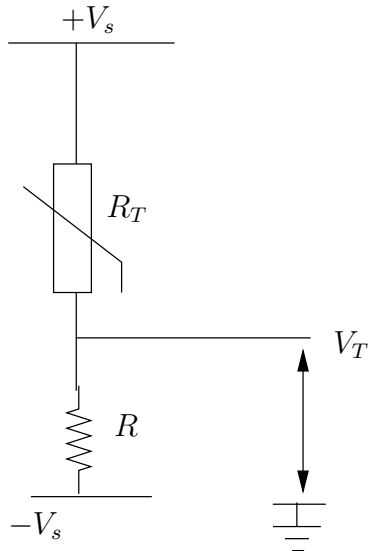


Figure 2: Voltage divider network used to monitor circuit ambient temperature changes.

## 2.1 Circuit Experiment

An experiment of the aforementioned circuit was performed with  $R_1 = 10k\Omega$  and the rest of the component values as shown in table 1. This was preferred because at  $R_1 = 1k\Omega$ , which corresponds to classical M-S parameter values, there was saturation in the OpAmps and Multipliers. The circuit was constructed on a bread board with off the shelf components. In particular, we used AD712J OpAmps and AD534 multipliers. These had internal trimming to counter potential offset problems due to temperature drift. In order to minimise ambient temperature effects, the circuit was encased in a metallic box which was then placed in a bigger insulated box prior to data collection.

The resistance  $R_7$  was varied and the circuit behaviour monitored using an oscilloscope. As  $R_7$  was varied between  $2.55k\Omega$  and  $5k\Omega$ , a rich array of bifurcations between periodic orbits and chaotic attractors was observed. In particular, periodic behaviour was observed in the intervals  $2.55k\Omega \leq R_7 \leq 2.60k\Omega$ ,  $2.65k\Omega \leq 2.70k\Omega$ . The main chaotic window for the circuit was found to be  $3.05k\Omega \leq R_7 \leq 3.85k\Omega$ . For  $R_7 > 3.85k\Omega$ , an interplay of periodic and chaotic behaviour was observed.

For the purposes of studying predictability when the dynamics were chaotic, we concentrated on the parameter  $R_7 = 3.85k\Omega$  (equivalently  $\gamma = 3.85$ ). The data was sampled at a frequency of 10kHz, each run lasting about 14 hrs. The circuit ambient temperature was monitored using a voltage divider network whose simplified version is shown in figure 2.  $R_T$  is a thermistor, a temperature dependent resistor which we attached to the body of the metal encasing (making sure that a good thermal contact was made),  $R$  is a fixed colour coded resistor,  $V_s$  is the supply DC voltage, and  $V_T$  is the voltage potential (relative to ground) at a point between  $R$  and  $R_T$ . Changes in ambient temperature were estimated by monitoring changes in  $V_T$  (Please refer to Appendix A for details).

The signals for  $V_T$  during the collection of two data sets are shown in figure 3.  $T_i = V_T^{(i)}$  is the temperature proxy corresponding to the  $i$ th collection. Notice that the maximum swing for  $T_7$  is  $-1V$ . Therefore, we can use (12) to get  $\Delta R_T = 20k\Omega$ , taking  $R = 100k\Omega$  and  $V_s = 10V$ . Substituting these values into (14) yields the maximum

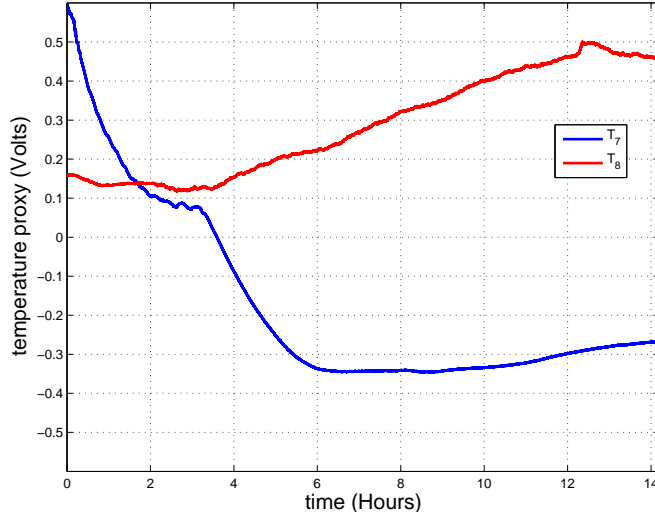


Figure 3: Smoothed temperature proxies for the long circuit data sets.  $T_7$  (for Set7) and  $T_8$  (for Set8) are the temperature proxies, with  $T_i = V_T^{(i)}$ . A rise in the each graph reflects increase in ambient temperature.

temperature change

$$\Delta T \approx 3.54^\circ C,$$

where we used  $T = 296K$ , the temperature at which the air-conditioner was set. Whether this temperature change affected circuit dynamics is a question we shall address later.

## 2.2 Numerical Simulations versus Circuit

The MS-system was integrated using the Matlab ordinary differential equations solver, ode45. To obtain a bifurcation transition sequence, the system was integrated with  $\gamma$  as the bifurcation parameter. For each value of  $\gamma \in [0, 5]$ , the initial conditions were selected randomly from a multivariate Gaussian distribution with zero mean and an identity covariance matrix. The system was then integrated over the time interval  $t \in [0, 4096]$ . Half of the signal was then ignored to eliminate transients. Extrema of the remaining signal of  $z$  were then plotted against  $\gamma$  to produce bifurcation transition sequences shown in figure 4.

According to the left graph, there is a small window within which chaos are manifest. The parameter region for this is  $\gamma \in (2.7, 3.9)$ . Outside this window, the M-S system yields a bifurcating sequence of periodic orbits. At  $\gamma = 3.85$ , the M-S attractor is predominantly periodic for any randomly selected initial condition. With a small chance, we can get the attractor shown on the left hand of figure 5, which is slightly reminiscent to the circuit attractor at the same parameter values. In accordance with model uncertainty, we can perturb one parameter to  $\delta = 1.3$  and keep  $\Gamma = 10$ . In this case, we obtain the bifurcation transition sequence shown on the right hand in figure 4. There are now chaotic windows, one at  $\gamma \sim 2.71$  and a wider one in the interval  $\gamma \in (3.05, 3.84)$ . A typical attractor corresponding to these parameters when  $\gamma = 3.81$  is shown on the right hand of figure 5. It shows greater likeness to the circuit attractor, which is shown on the bottom of the same figure.

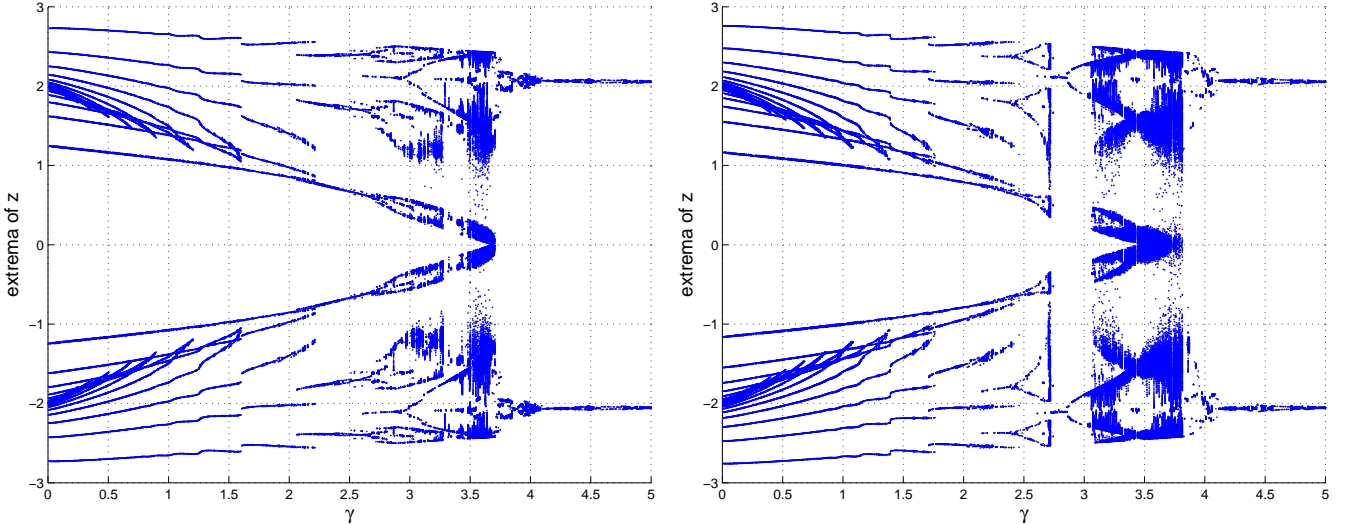


Figure 4: Bifurcation transition sequences for the M-S system corresponding to  $\delta = 1$  (left) and  $\delta = 1.3$  (right), both with  $\Gamma = 10$ .

There are clear differences between the M-S system and the circuit at the parameter values considered. Parameter values that yield the closest behaviour of the M-S system to the circuit could be elicited by a systematic inverse problem approach. Fixing  $\delta = 1$ , parameters that minimise forecasting error (see appendix B for details of the forecasting error statistic) at a lead time of  $\tau = 12.8$  ms over 512 initial conditions were found to be  $\gamma = 3.524$  and  $\Gamma = 7.888$ . At this set of parameter values, the dynamics always settle on a limit cycle. The overall differences in the attractors need not forbid us from forecasting the circuit with the M-S system. It has indeed been highlighted in [7] that agreement in behaviour between a model and corresponding system is not necessary, although sufficient, for good forecasting performance. In fact, forecasting the circuit from eight initial conditions using the M-S system indicates that the forecasts track the M-S system well for about half an oscillation (see figure 6). This is with the exception of just a few initial conditions where the forecast trajectory goes astray very quickly.

### 3 Predictability

This section briefly outlines the framework for discussing the predictability of the circuit. It goes further to draw the implications of Takens theorem when the underlying model is imperfect. It is argued that regional predictability variations are a function of the model coordinate space in the perfect model scenario.

#### 3.1 Initial Uncertainty Growth Times

Consider a model of a physical system given by:

$$\dot{\mathbf{x}} = \mathbf{F}(\mathbf{x}(t)), \quad (4)$$

where  $\mathbf{x}, \mathbf{F} \in \mathbb{R}^m$ . Then the dynamics of an infinitesimally small uncertainty are governed by

$$\dot{\boldsymbol{\epsilon}} = \mathbf{J}(\mathbf{x})\boldsymbol{\epsilon},$$

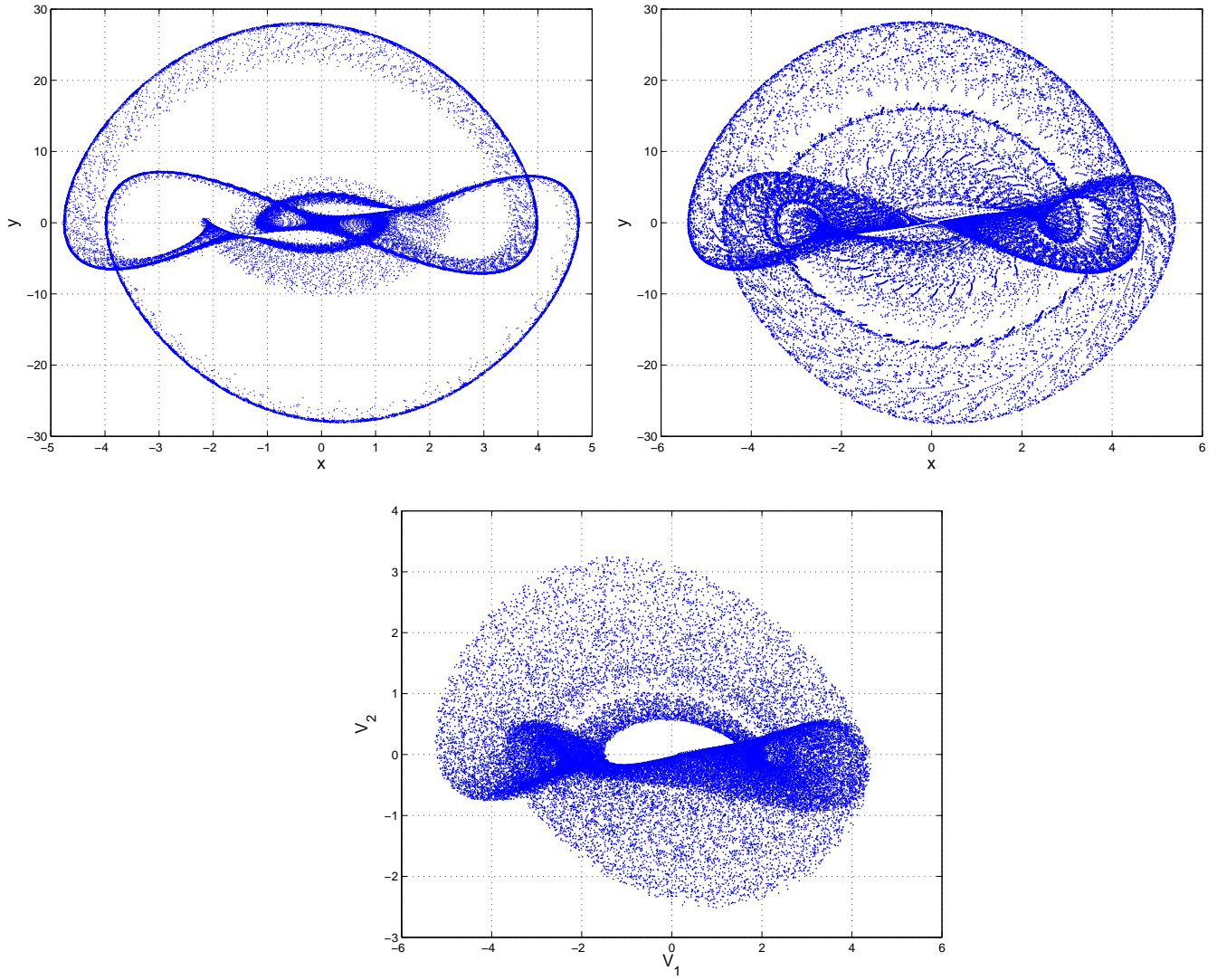


Figure 5: Chaotic attractors for the MS system at  $(\delta, \gamma) = (1, 3.85)$  (top left) and  $(\delta, \gamma) = (1.3, 3.81)$  (top right) with  $\Gamma = 10$ . On the bottom is the circuit attractor.

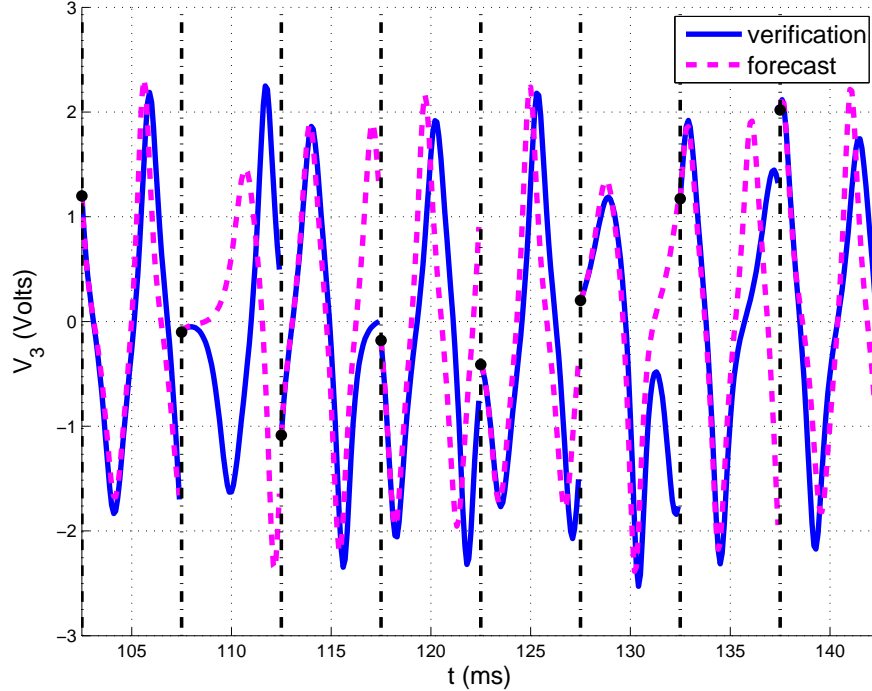


Figure 6: Forecasts of the circuit from 8 initial conditions using the M-S system at parameter values  $\delta = 1.3$ ,  $\gamma = 3.81$  and  $\Gamma = 10$ . The black dots correspond to the initial conditions.

where  $J(\mathbf{x})$  is the Jacobian of  $\mathbf{F}$  at  $\mathbf{x}$ . If  $\epsilon_0$  is the initial uncertainty at  $\mathbf{x}_0$  and  $\varphi(\mathbf{x})$  is the solution to (4), then the  $q$ -pling time is defined as [1]

$$\tau_q(\epsilon, \mathbf{x}_0) = \inf \{t \mid \|\varphi_t(\mathbf{x} + \epsilon_0) - \varphi_t(\mathbf{x})\| \geq q\|\epsilon_0\|\}.$$

When  $q = 2$ , we have the doubling time and when  $q = 4$  we have the quadrupling time.

We can also think of the dynamics of an initial uncertainty as being governed by the linear propagator [8],

$$\mathcal{M}(\mathbf{x}_0, \Delta t) = \exp \left( \int_{t_0}^{t_0 + \Delta t} D_{\mathbf{x}} \mathbf{F} dt \right).$$

It maps  $\epsilon_0$  to  $\epsilon(t)$  via

$$\epsilon_0(t_0 + \Delta t) = \mathcal{M}(\mathbf{x}_0, \Delta t) \epsilon_0.$$

The singular value decomposition of  $\mathcal{M}$  is  $\mathcal{M} = U \Sigma V^T$  with orthogonal matrices  $V$  ( $U$ ) containing the right (left) singular vectors as columns and  $\Sigma$  the diagonal matrix of the singular values,  $\sigma_i$  with  $\sigma_i \geq \sigma_j$  for  $i < j$ .

At a fixed location,  $\mathbf{x}_0$ , the *Lyapunov vector* is determined from the singular value decomposition of  $\lim_{\Delta t \rightarrow -\infty} \mathcal{M}(\mathbf{x}_0, \Delta t)$  [1, 9]. Then the Lyapunov direction (Lyapunov vector),  $\mathbf{u}_1$ , is the first column of  $U$  [1].

### 3.2 Implications of Takens

Essentially, Takens' theorem [10] states conditions under which a measurement function  $h$  yields, with probability one, a coordinate function  $\mathbf{H}$  which is a differentiable embedding [8]. This affords us the benefit of moving into another coordinate space and yet

preserve ergodic measures [8, 10, 11]. To see this, let  $\varphi_t$  denote the dynamical flow on some manifold. Then the flow on the reconstructed manifold is given by

$$\phi_t = \mathbf{H}\varphi_t\mathbf{H}^{-1}. \quad (5)$$

Applying the chain rule to equation (5) yields [8]

$$D\phi_t = D\mathbf{H}D\varphi_tD\mathbf{H}^{-1},$$

which implies that the matrices  $D\phi_t$  and  $D\varphi_t$  are similar [8, 12] with the similarity transformation being  $D\mathbf{H}$ . It then follows that the eigenvalues of  $D\varphi_t$ , denoted by  $\lambda(D\varphi_t)$ , are contained in those of  $D\phi_t$ , denoted by  $\lambda(D\phi_t)$  [12]. In capsule form,

$$\lambda(D\varphi_t) \subseteq \lambda(D\phi_t). \quad (6)$$

Although (6) guarantees the preservation of global quantities like Lyapunov exponents, it places no restriction on local measures of predictability. This, in turn, means instantaneous time measures in the embedding space may be different from those in the system state space. This will inevitably be true when our models are imperfect. The third contributing factor is the presence of "spurious" exponents (eigenvalues/singular values) that creep in when we move into embedding space.

Consider the vector  $\mathbf{X}_n$  used to compute the q-pling times. This may be related to the delay vector  $\mathbf{x}_n$  by the mapping:

$$\mathbf{G} : \mathbf{X}_n \rightarrow \mathbf{x}_n.$$

This mapping is clearly one to one. If the dynamics of  $\mathbf{X}_n$  are governed by  $\Phi_t$ , the flow on the delay space is governed by  $\mathbf{G}\Phi_t$  and this leads to the relation

$$\mathbf{G}\Phi_t = \mathbf{H}\varphi_t\mathbf{H}^{-1}. \quad (7)$$

whence the chain rule yields

$$D\mathbf{G}D\Phi_t = D\mathbf{H}D\varphi_tD\mathbf{H}^{-1}. \quad (8)$$

From equation (7), we cannot conclude that  $\Phi_t$  and  $\varphi_t$  are isomorphic and (8) does not guarantee similarity between  $D\Phi_t$  and  $D\varphi_t$ . This means that if one has two models, one in delay space and another in system state space, the variations in predictability will inevitably be different.

## 4 RBF Models

In section 2, it was evident that the M-S system fails badly to forecast the circuit from some initial conditions. A natural alternative to address the forecasting problem when the dynamics are low dimensional is to appeal to RBFs. When constructed for forecasting, RBF models may fail to faithfully capture the attractor of the underlying system. Nevertheless, they offer significant improvement where the M-S system fails and can even do better at other initial conditions where the M-S system forecasts the circuit fairly well.

In order to construct RBF models for the circuit, we followed [13] without concerning ourselves with the minimum description length criterion therein. The variable of interest

Model	No. of RBFs	Dimension ( $m$ )	Coordinate space
$M_1$	40	3	Delay
$M_2$	40	4	Delay
$M_3$	25 per var	3	state space
$M_4$	40	3	Delay

Table 2: The table of models of the circuit that were built using cubic radial basis functions (RBF). In the second column, per var stands for per measurement variable. Models with the same coordinate space are different because they have different centres and RBF coefficients.

was  $V_3$  (resp.  $z$ ) because of its correspondence to the height of an ionised gas in the atmosphere of a star as discussed in [5]. Some of the models were based on the single variable, in which case delay embedding reconstructions were used. The other approach was to use all the three variables to construct the models, which effectively meant multiple models were built to forecast each variable separately. At every iteration step, there would then be three models to run forward. In both cases, finding an RBF model was treated as an interpolation [13, 14].

For models constructed from the  $V_3$  signal alone, suppose that  $\mathbf{x}$  is some corresponding delay vector and construct the model  $\phi(\mathbf{x}) : \mathbb{R}^m \rightarrow \mathbb{R}$ , which takes the form

$$\phi(\mathbf{x}) = \sum_{j=1}^{n_c} \lambda_j \psi(\|\mathbf{x} - \mathbf{c}_j\|) + L(\mathbf{x}), \quad (9)$$

where  $\psi(r)$  are radial basis functions,  $\lambda_j$  are constants determined by observations in the learning set so that

$$\phi(\mathbf{x}_i) = s_{i+1}, \quad (10)$$

and  $L(\mathbf{x})$  are linear terms. The vectors  $\mathbf{c}_j$  are the associated centres. Cubic RBFs used were of the form  $\psi(r) = r^3$ . An appropriate time delay was chosen via the mutual information criterion [15].

On the other hand a state space model takes the form

$$\mathbf{x}_{n+1} = \phi(\mathbf{x}_n), \quad (11)$$

where  $\phi$  is a vector whose components are linear combinations of RBFs. That is  $\phi = (\phi_1, \phi_2, \dots, \phi_m)^T$  with

$$\phi_i(\mathbf{x}) = \sum_{j=1}^n \lambda_{ij} \psi(\mathbf{x} - \mathbf{c}_{ij}) + L_i(\mathbf{x})$$

where  $\mathbf{c}_{ij}$  are the centres and  $L_i$  are linear terms.

A table of RBF models of the circuit is given in table 2. These were used to make predictions of predictability of the circuit as discussed in the next section.

## 5 Results

This section presents the results of computations of uncertainty quadrupling times from different initial conditions of the circuit. Only Lyapunov directions are considered. We

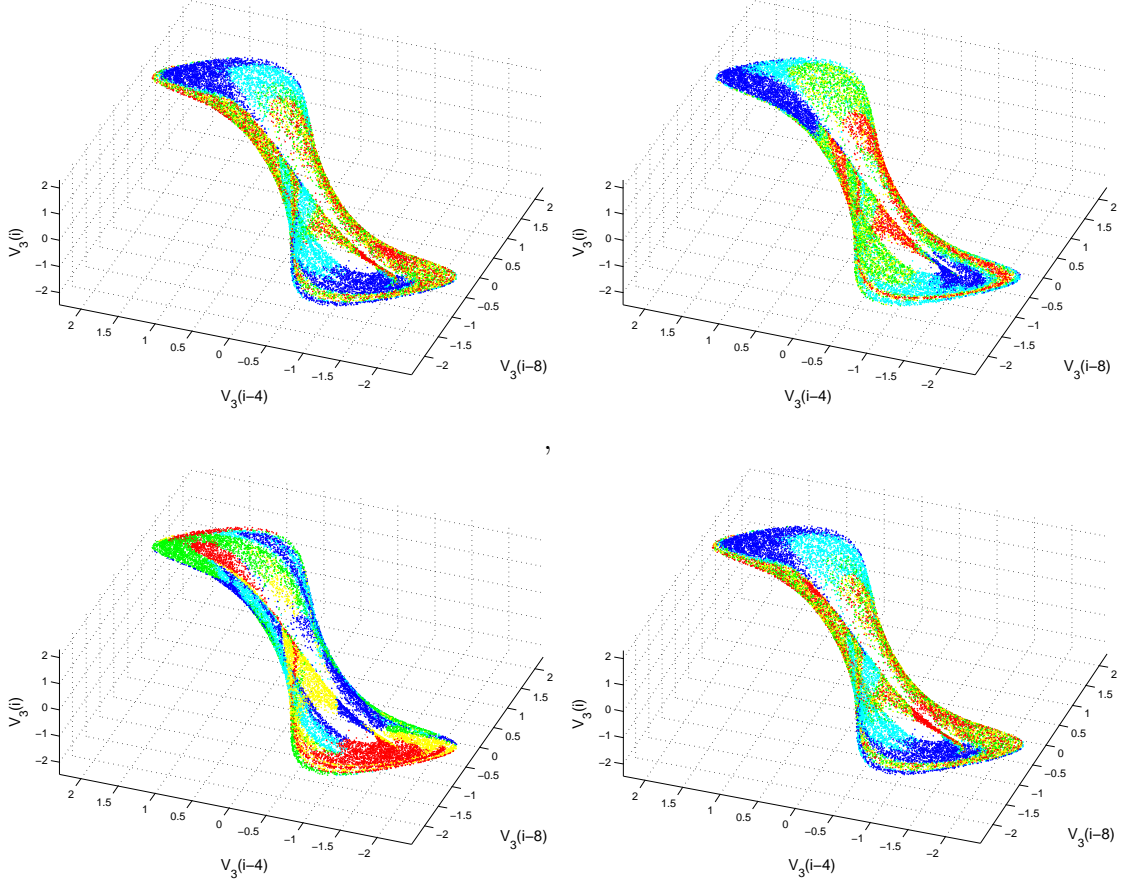


Figure 7: *Distributions of quadrupling times for models (a)  $M_1$ , (b)  $M_2$ , (c)  $M_3$  and (d)  $M_4$  of the circuit. Models  $M_1$  and  $M_4$  were built in 3D delay space, model  $M_2$  in 4D delay space and model  $M_3$  in measurement space (or state space). From measurement space, the distribution of quadrupling times for model  $M_3$  were then mapped into delay space. Red indicates  $F(\tau_4) < 0.2$ , yellow indicates  $0.2 < F(\tau_4) < 0.4$ , green indicates  $0.4 < F(\tau_4) < 0.6$ , cyan indicates  $0.6 < F(\tau_4) < 0.8$  and blue indicates  $F(\tau_4) > 0.8$ .  $F(\cdot)$  is the cumulative distribution function of the quadrupling times.*

consider growth of initial uncertainties under the dynamics of the RBF models of table 2. The models were constructed in different coordinate spaces.

Distributions of quadrupling times of initial uncertainties under each model are shown in figure 7. To aid comparison, all model spaces have been projected onto 3D delay space. It turns out that 3D delay space models,  $M_1$  and  $M_4$ , exhibit the most similar estimates of predictability distributions. Note that these two models are different because their centres and RBF coefficients differ. The model in 3D state space exhibits the least similarity to the other models in delay space.

A table of values of the similarity measure for uncertainty quadrupling time distributions for these models is shown in table 3. Details of the similarity measure can be found in appendix C. Notice that  $l(\Gamma_s^{(M_1, M_4)}) = 0.9103$ , and is the highest value. Next in magnitude is  $l(\Gamma_s^{(M_2, M_4)}) = 0.3435$ . These results support the conclusion that the greatest similarity is exhibited by models  $M_1$  and  $M_4$ , which were built in 3D delay

Model	$M_1$	$M_2$	$M_3$	$M_4$
$M_1$	1	0.332	0.1458	0.9103
$M_2$	0.332	1	0.1583	0.3435
$M_3$	0.1458	0.1583	1	0.1323
$M_4$	0.9103	0.3435	0.1323	1

Table 3: Table of values of  $l(\Gamma_s^{(i,j)})$ , the similarity measure, for the models indicated on the first column and first row of the table whose quadrupling time distributions.  $\Gamma_s^{(i,j)}$  is the similarity set for model  $i$  versus model  $j$  and  $l$  is some measure (see appendix C). According to this table, all the models in delay space exhibit the least similarity to model  $M_3$  (model in state space).

space, followed by similarity between these two with model  $M_2$ , another delay space model. Model  $M_3$  manifests the least similarity to the rest of the models.

It seems that these similarities and differences are largely due to differences in modelling spaces rather than model error. Comparing predictions of predictability for the RBF model in state space with those for the M-S system yields a very low value of the similarity measure for the quadrupling times. In fact, quadrupling time distributions for the M-S system (not shown) manifest no greater similarity to the RBF model in state space than they do to the delay space models. Thus we conclude that the observed inter-model predictability differences are a property of the RBF models constructed according to [13]. A discussion of these results continues in § 6.

Since we present this circuit as a possible test-bed for different aspects of signal processing and complexity studies, the reader might have questions about the stability of the dynamics under drifting temperature. To settle this concern, we computed predictability estimates of the circuit under different temperature regimes. Distributions of quadrupling times under model  $M_3$  for Set1 are shown in figure 8. The left and right graphs correspond to the dynamics at the beginning and end of collection, respectively. The striking similarity is evidence that the dynamics were stable over the observation period.

## 6 Discussion

Circuit realisations and the M-S system showed some agreement in the general behaviour, which appeared to be in a topological sense. Techniques similar to those employed in [16] could be used to make a rigorous topological comparison. Since our interest is forecasting, such an approach would not be of much value in the present context. We note, however, that a lot of the literature that compares digital and analogue signals tend to rely solely on a visual inspection (e.g. see [17, 18, 19]). A comparison of analogue and digital realisations via a forecasting approach seems to be a novel feature in this paper.

Notwithstanding the similarities between the circuit and the M-S system by visual inspection of the attractors, there are apparent disparities. The parameter values at which the M-S system yields an attractor that is similar to the circuit attractor differ from those inferred from the circuit component values. Such a phenomenon is reminiscent to that observed in [17], who argued that it could be due to parametric uncertainty. Moreover, just like the case reported here, the analogue and digital attractors reported in [17] do not exhibit perfect similarity. The point is that the problems identified with

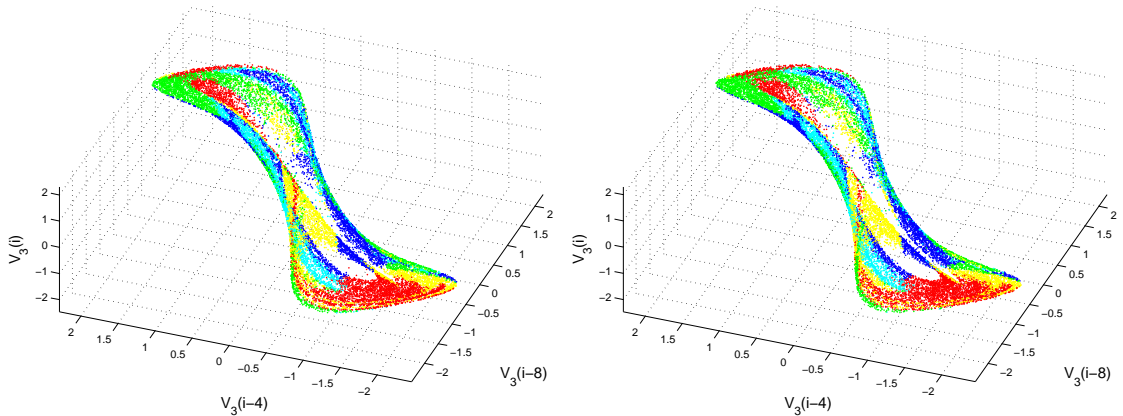


Figure 8: Views of the MS circuit showing distributions of quadrupling times for model  $M_3$  of the circuit on data at the beginning and end of Set1. Red indicates  $F(\tau_4) < 0.2$ , yellow indicates  $0.2 < F(\tau_4) < 0.4$ , green indicates  $0.4 < F(\tau_4) < 0.6$ , cyan indicates  $0.6 < F(\tau_4) < 0.8$  and blue indicates  $F(\tau_4) > 0.8$ .  $F(\cdot)$  is the cumulative distribution function of the quadrupling times. The similarity between these two pictures suggests that the circuit dynamics are not altered by the ambient temperature fluctuations.

the modelling of the circuit by the M-S system are not a singularity. It might be that the M-S system cannot adequately describe the circuit. As a model of the circuit, the M-S system is obtained by making ideal component assumptions. In reality, non of the components is ideal. The cumulative effect of many non-ideal components can invalidate this assumption. It is not surprising, therefore, that Luchisky et al. [20] recommend using the minimum possible number of active components in the design of an analogue circuit. This “minimum” may be too much for a Kirchoff based model to adequately describe the underlying circuit. Although often less appreciated, model inadequacy is a ubiquitous feature in the applied sciences.

Various perturbations of the M-S system’s parameters yielded a system that either settled on a periodic orbit or simply did not exactly resemble the circuit attractor. In fact, the M-S system tended to fail in the same way to forecast the circuit from some of the initial conditions. For this reason, we conclude that the disparity between the M-S system is mainly due to model inadequacy rather than parametric uncertainty. Therefore, an RBF approach was used to characterise the circuit dynamics. Just like neural networks, it has been argued that RBFs can be used to describe a nonlinear dynamical system [13]. We found it interesting that RBF models constructed in the same coordinate space yielded very similar distributions of predictability estimates. Such models could be viewed as an attempt to capture parametric uncertainty. The foregoing discussion suggests that parametric perturbations could give one a false confidence on their predictability estimates. It is helpful to use different model classes.

The results of this work may be useful in Meteorology, where the growth of initial uncertainty has received particular attention. A major inhibiting factor in studying uncertainty growth directly on the climate system is computational complexity and operational challenges. As reported in [21], toy examples are often resorted to in order to unravel the distribution of uncertainty over a chaotic system. The examples tend to focus

on the perfect model scenario. Nonetheless, the ECMWF appreciates the problems posed by model imperfection. At ECMWF, forecasts from a sample of initial conditions are made by an ensemble of models. The models are apparently parametric perturbations of a single model [21, 22], which may not adequately explore uncertainty. It is advisable to adopt a multiple model class approach. Indeed we have demonstrated that fairly good forecasting model classes can yield conflicting predictability distributions. This is a step further than previous toy examples (e.g. see [1, 21]) that ended only in the perfect model scenario. The results undermine the notion, set forth by Kalnay et al. [2], that regional losses in predictability are an indication of the instability of the underlying flow.

The results also motivate further the need to use multiple model classes in forecasting. Since the pioneering work of Granger and Ramanathan [23], the use of multiple models found favour in the economics community. Current discussion is now focusing on combining density forecasts (e.g. see [24, 25]). Within the past decade, climate scientists have started to consider the use of multiple models with particular emphasis on seasonal weather forecasts [26, 27, 28]. This is very much welcome because unlike in linear models of economics, the predictability of the climate system varies with regions in state space.

This work also highlights an important aspect of RBF models. It is evident that we can increase inter-model variation by constructing the models in various coordinate spaces. The effect of this is to provide an ensemble of model classes to account for model uncertainty. It is obvious that it makes no sense to combine models that agree in behaviour across an attractor. Therefore, if one wants to combine RBF models, it is a good idea to construct them in different coordinate spaces.

## 7 Conclusions

This paper presented an electronic circuit which can be used as a test-bed for time series analysis techniques for different real world applications. The circuit may also be seen as a contribution to the literature on chaotic circuits. Unlike most chaotic circuits that appear in the literature, the circuit has a non-linearity of degree three. Even though the observation period spanned over fourteen hours, appealing to uncertainty growth times, it was established that the dynamics remain stable. Despite the similarities between the circuit and the corresponding M-S model, we are clearly in the imperfect model scenario. This situation should not raise an alarm because imperfect models are ubiquitous in the real world.

The ultimate limit to predicting predictability is model inadequacy. It impacts both our ability to capture the initial uncertainty and how that uncertainty evolves over time. Whereas good forecasting performance by a particular model could tempt one to use it to make estimates of predictability across the underlying system, it was demonstrated with multiple models that model inadequacy makes that illusive. On a positive note, the variations in predictability estimates by the different model classes are a case for multiple model approach to forecasting. In the case of RBF models, inter-model variation could be maximised by constructing them in different coordinate spaces and/or basis functions.

## Acknowledgements

The author would like to thank Devin Kilminster and the New Zealand Met Service for his useful insights and for writing the code used to access the data. I appreciate

useful discussions with members of the Applied Dynamical Systems and Inverse Problems Group at the University of Oxford. This work was supported by the RCUK digital economy programme at the University of Reading.

## References

- [1] L. A. Smith, C. Ziehman, K. Fraedrich, Uncertainty in dynamics and predictability in chaotic systems, *Q. J. R. Meteorol. Soc.* 125 (1999) 2855–2886.
- [2] E. Kalnay, M. Corazza, M. Cai, Are Bred Vectors the same as Lyapunov Vectors, *Symposium on Observations, Data Assimilation, and Probabilistic Prediction (2002)* 173–177.
- [3] V. M. Khade, J. A. Hansen, State dependent predictability: Impact of uncertainty dynamics, uncertainty structure and model inadequacies, *Nonlinear Processes in Geophysics* 11 (2004) 351–362.
- [4] P. E. McSharry, L. A. Smith, Consistent nonlinear dynamics: identifying model inadequacy, *Physica D* 192 (2004) 1–22.
- [5] W. D. Moore, E. A. Spiegel, A thermally excited nonlinear oscillator, *The Astrophysical Journal* 143 (1966) 871–887.
- [6] N. J. Balmforth, R. V. Craster, Synchronizing Moore and Spiegel, *Chaos* 7 (1997) 738:752.
- [7] D. Kilminster, R. L. Machete, Prediction, behaviour, ignorance, *NOLTA* (2005).
- [8] E. Ott, T. Sauer, J. Yorke, *Coping With Chaos: Analysis of chaotic data and the exploitation of chaotic systems*, John Wiley and Sons, Inc. New York, 1994.
- [9] C. Ziehmann, L. A. Smith, K. Fraedrich, Localised lyapunov exponents and the prediction of predictability, *Phys. Rev. Lett.* 271 (1999) 237–251.
- [10] F. Takens, *Detecting strange attractors in turbulence*, Springer-Verlag, 1981.
- [11] J.-P. Eckmann, D. Ruelle, Ergodic theory of chaos and strange attractors, *Rev. Mod. Phys.* 57 (1985) 617–653.
- [12] G. H. Golub, C. F. Loan, *Matrix Computations*, 3rd Edition, The John Hopkins University Press, 1996.
- [13] K. Judd, A. Mees, On selecting models for nonlinear time series, *Physica D.* 82 (1995) 426–444.
- [14] I. R. H. Jackson, Convergence Properties of Radial Basis Functions, *Constructive Approximation* 4 (1988) 243–264.
- [15] A. M. Fraser, H. L. Swinney, Independent coordinates for strange attractors from mutual information, *Physical Review A* 33 (1986) 1134.
- [16] I. M. Moroz, C. Letellier, R. Gilmore, When is a projection an embedding?, *Physical Review E* 75.

- [17] R. Kilic, O. G. Saracoglu, F. Yildirim, A new nonautonomous version of Chua’s circuit: Experimental observations, *Journal of the Franklin Institute* 343 (2006) 191–203.
- [18] M. E. Yalcin, J. A. K. Suykens, J. Vandewalle, Experimental Confirmation of 3- and 5-Scroll Attractors from a Generalized Chua’s Circuit, *IEEE Transactions on Circuits and Systems-I: Fundamental Theory and Applications* 47 (2000) 425–429.
- [19] G. Mayer-Kress, I. Choi, N. Weber, R. Bargar, A. Hubler, Musical Signals from Chua’s Circuit, *IEEE Transactions on Circuits and Systems-II: Analog and digital signal processing* 40 (1993) 688–695.
- [20] D. G. Luchisky, P. V. E. McClintock, M. I. Dykman, Analogue studies of nonlinear systems, *Reports on Progress in Physics* 61 (1998) 889–997.
- [21] T. N. Palmer, Predicting uncertainty in forecasts of weather and climate, *Reports on Progress in Physics* 63 (2000) 71–116.
- [22] T. N. Palmer, R. Buizza, F. Doblas-Reyes, T. Jung, M. Leutbetcher, G. J. Shutts, M. Steinheimer, A. Weisheimer, Stochastic parametrisation and model uncertainty, Tech. Rep. 598, European Centre for Medium-Range Weather Forecasts (October 2009).
- [23] C. W. Granger, R. Ramanathan, Improved methods of combining forecasts, *Journal of Forecasting* 3 (1984) 197–204.
- [24] S. G. Hall, J. Mitchell, Combining density forecasts, *International Journal of Forecasting* 23 (2007) 1–13.
- [25] C. Kascha, F. Ravazzolo, Combining Inflation Density Forecasts, *Journal of Forecasting* 29 (2010) 231–250.
- [26] T. N. Palmer, F. J. Doblas-Reyes, R. Hagedorn, A. Weisheimer, Probabilistic prediction of climate using multi-model ensembles: from basic to applications, *Phil. Trans. R. Soc. B* 360 (2005) 1991–1998.
- [27] T. N. Palmer, G. J. Shutts, R. Hagedorn, F. J. Doblas-Reyes, T. Jung, M. Leutbetcher, Representing Model Uncertainty in Weather and Climate Prediction, *Annu. Rev. Earth Planet. Sci.* 33 (2005) 163–193.
- [28] A. W. Robertson, U. Lall, S. E. Zebiak, L. Goddard, Improved Combination of Multiple Atmospheric GCM Ensembles for Seasonal Prediction, *Monthly Weather Review* 132 (2004) 2732–2744.
- [29] J. S. Steinhart, S. R. Hart, Calibration curves for thermistors, *Deep Sea Res.* 15 (1968) 497–503.

## A Ambient Temperature Monitoring

It follows from Kirchhoff’s laws that

$$V_T = \frac{(R - R_T)}{R + R_T} V_s.$$

Changes in the ambient temperature were then monitored by monitoring changes in  $V_T$  because  $V_s$  and  $R$  are fairly stable. In fact, to first order approximation,

$$\Delta R_T = -2R \frac{V_s \Delta V_T}{(V_T + V_s)^2}. \quad (12)$$

Over a small range of temperatures, the thermistor may be assumed to vary linearly with temperature according to

$$\Delta R_T = k \Delta T,$$

where  $k$  is a constant, called *temperature coefficient*. If  $k$  is positive, then the thermistor is said to have a positive temperature coefficient. If  $k$  is negative, it is said to have a negative temperature coefficient. Over a wide range of temperatures, the Steinhart equation [29] is more appropriate and a special form of it is given by

$$R_T = R_{T_0} \exp \left[ \frac{\beta(T_0 - T)}{T_0 T} \right], \quad (13)$$

where  $T_0$  is some standard temperature,  $R_{T_0}$  is the resistance of the thermistor at  $T_0$ . The temperature is in Kelvin and  $T_0$  is usually  $298.15K$ . The thermistor used was an NTC with  $R_{T_0} = 100k\Omega$ ,  $T_0 = 298.15K$  and  $\beta = 4450$ .

To get an idea of the underlying temperature fluctuations, we need to transform a given voltage change. Equation (13) may be rearranged into

$$T = \left[ \frac{1}{\beta} \ln \left[ \frac{R_T}{R_{T_0}} \right] + \frac{1}{T_0} \right]^{-1},$$

from which we get

$$\begin{aligned} \Delta T &\approx \frac{\partial T}{\partial R_T} \Delta R_T \\ &= - \left[ \frac{1}{\beta} \ln \left[ \frac{R_T}{R_{T_0}} \right] + \frac{1}{T_0} \right]^{-2} \frac{\Delta R_T}{\beta R_T}. \end{aligned} \quad (14)$$

## B Parameter Estimation

Given some data and a model of the system, a common problem is to estimate the best parameters according to some criterion. In particular, we can seek parameters that minimise forecast errors in the Euclidean norm. For a given time series of initial states,  $\{\mathbf{s}_t\}_{t \geq 1}$ , the error to minimise is:

$$E_T(\tau) = \frac{1}{\tau(T - \tau)} \int_0^{T-\tau} \int_t^{t+\tau} \|\mathbf{s}_s - \phi(\mathbf{s}_t, w - t)\| dw dt, \quad (15)$$

where  $\tau$  is the forecast lead time,  $T$  is the duration of the observation period and  $\phi$  is the underlying model flow with the property that  $\phi(\mathbf{s}_t, 0) = \mathbf{s}_t$ . The flow  $\phi$  may be obtained via numerical integrations.

## C Similarity Measure

It is crucial that we find a measure to compare distributions of q-pling times across an attractor. In order to define such a measure, consider two models,  $M_1$  and  $M_2$  with q-pling times  $\tau_q^{M_1}$  and  $\tau_q^{M_2}$  respectively. Let  $\tau_q^{M_i} = \tau_q^{M_i}(t)$  be the q-pling time of model  $M_i$  at a point realised on the attractor at time  $t$ . Suppose the cumulative distribution function for the q-pling times of model  $M_i$  is  $F_i(\tau_q^{M_i})$ . If we partition each  $F_i$  with points  $\{p_j\}_{j=0}^n$  with  $p_0 = 0$  and  $p_n = 1$ , we can then define the  $j$ th q-pling time similarity set of the two sets of q-pling times by

$$\Gamma_s^j = \{(\tau_q^{M_1}(t), \tau_q^{M_2}(t)) : F_1(\tau_q^{M_1}(t)), F_2(\tau_q^{M_2}(t)) \in [p_{j-1}, p_j]\}.$$

Whence the global similarity set, which depends on the partition  $\{p_j\}_{j=0}^n$ , is defined as

$$\Gamma_s^{(M_1, M_2)} = \bigcup_{j=1}^n \Gamma_s^j.$$

If  $l$  is a probability measure defined on the universal set containing  $\Gamma_s^{(M_1, M_2)}$ , the similarity between the q-pling time distributions for the two models will be  $l(\Gamma_s^{(M_1, M_2)})$ , where

$$l(\Gamma_s^{(M_1, M_2)}) = \lim_{T \rightarrow \infty} \frac{1}{T} \int_0^T \mathbf{1}_{\Gamma_s^{(M_1, M_2)}}(\mathbf{x}(t)) dt$$

and  $\mathbf{x}(t)$  is the system trajectory in state space. The corresponding finite approximation over a discrete set of observations  $\{\mathbf{s}_i\}_{i=1}^N$  is

$$l(\Gamma_s^{(M_1, M_2)}) \approx \frac{1}{N} \sum_{i=1}^N \mathbf{1}_{\Gamma_s^{(M_1, M_2)}}(\mathbf{s}_i),$$

where  $\mathbf{s}_i = \mathbf{h}(\mathbf{x}_i)$ ,  $\mathbf{x}_i = \mathbf{x}(i\tau_s)$ ,  $\mathbf{h}$  is some observation function and  $\tau_s$  is the sampling time.

A few observations are worth mentioning. To this end, let  $M_3$  be a third model with q-pling times  $\bigcup_{t \geq 0} \{\tau_q^{M_3}(t)\}$ .

- If for some predefined  $\epsilon > 0$ ,

$$1 - \epsilon < l(\Gamma_s^{(M_1, M_2)}) \leq 1, \tag{16}$$

we say that model  $M_1$  is similar to model  $M_2$  up to  $\epsilon$  and the partition in question. For a given partition, greater similarity between q-pling time distributions of two models across the attractor is reflected by smaller  $\epsilon$ .

- Inequality (16) effectively defines an equivalence relation between models. Indeed, if we alternatively write (16) as  $M_1 \sim M_2$ , the reflexivity, symmetry and transitivity properties follow in a pretty straight forward way <sup>2</sup>.

- If for a given partition

$$l(\Gamma_s^{(M_1, M_2)}) > l(\Gamma_s^{(M_1, M_3)}),$$

we say that model  $M_1$  has q-pling times distribution more similar to that of model  $M_2$  than to model  $M_3$  on the attractor in question.

---

<sup>2</sup>An equivalence relation satisfies reflexivity,  $M_1 \sim M_1$ , symmetry, which is  $M_1 \sim M_2 \Rightarrow M_2 \sim M_1$  and transitivity which is,  $M_1 \sim M_2$  and  $M_2 \sim M_3$  implies  $M_1 \sim M_3$ .